Inorganic Chemistry

Article

pubs.acs.org/IC

Syntheses, Characterization, and Optical Properties of Ternary Ba−Sn−S System Compounds: Acentric $Ba_7Sn_5S_{15}$, Centric $BaSn_2S_5$, and Centric $Ba_6Sn_7S_{20}$

Zhong-Zhen Luo,[†,‡] Chen-Sheng Lin,[†] Wen-Dan Cheng,*[,†] Hao Zhang,[†] Wei-Long Zhang,[†] and Zhang-Zhen He[†]

[†]State Key Laboratory of Structural Chemistry, Fujian Institute of Research on the Structure of Matter, Chinese Academy of Sciences, Fuzhou 350002, People's Republic of China

[‡]Graduate School of the Chinese Academy of Sciences, Beijing, 100039, People's Republic of China

Supporting Information

ABSTRACT: Three new ternary Ba−Sn−S system compounds, acentric $Ba_7Sn_5S_{15}$, centric $BaSn_2S_5$, and centric $Ba_6Sn_7S_{20}$ have been designed and synthesized by a conventional high-temperature solid-state reaction method using the evacuated silica tubes. The crystal structure of $Ba_7Sn_5S_{15}$ shows the coexistence of a SnS_4 tetrahedral and a Sn_2S_3 trigonal bipyramid. Importantly, the larger dipole moment of the $[Sn_2S_3]^{2-}$ trigonal bipyramid group and the polarity enhancement of the bipyramidal arrangements result in a strong SHG effect at 2.05 μm, which is 10 times of the SHG intensity of the benchmark $AgGaS_2$ with the particle size of 30−46 μm and twice as much as that with the particle size of 150−212 μm. Evidently, the acentric $Ba_7Sn_5S_{15}$ is a novel IR NLO crystal material with a wide mid-IR window and a strong SHG effect, which is the first reported among the Ba−Sn−S ternary system. Moreover, $Ba_7Sn_5S_{15}$ can achieve type-I phase-matching that can be used for practical applications. In the centric $BaSn_2S_5$, all Sn atoms are coordinated by five S atoms to form novel SnS_5 trigonal bipyramid polyhedrons. In the other centric $Ba_6Sn_7S_{20}$, there is the coexistence of the two coordination patterns with a SnS_5 trigonal bipyramid and SnS_4 tetrahedral polyhedrons, featuring a special crystal structure in the Ba−Sn−S system.

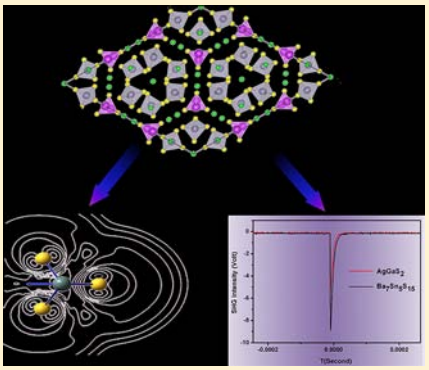

INTRODUCTION

Nonlinear optical (NLO) materials have gained tremendous interest in the mid-IR (2−20 μm)[1] applications, such as molecular spectroscopy, noninvasive medical diagnostics, environmental monitoring, deep-space detectors, space telescopes, infrared countermeasures, etc., and military and civilian systems.[2−5] However, only a few NLO crystals in the mid-IR crystals, such as $AgGaS_2$, $AgGaSe_2$, and $ZnGeP_2$, are commercially available so far. These materials obstruct further improvement of the laser power due to a low laser damage threshold, and no wide transparency in the mid-IR region.[6−8] Accordingly, we desire to gain new NLO materials with a wide IR window and high laser damage. However, it is a great challenge to design new IR crystal materials with a present function of SHG. A general strategy suggested is to employ noncentrosymmetric (NCS) chromophores as building units in the syntheses of NLO materials.[9−11] Up to now, among the NLO materials containing a chalcogenide element, most of them contain the tetrahedral structure unit.[12−17] Inspired by the reported results, we selected the NCS Sn tetrahedral or triangular coordination as building units to design and synthesize new NLO materials. In the present work, we obtained one NCS compound with the coexistence of Sn tetrahedral and trigonal pyramidal coordination among the syntheses of ternary Ba−Sn−S systems. We will present the synthesis, crystal structures, band structures, and NLO property of the compound $Ba_7Sn_5S_{15}$. Two new centric compounds, $BaSn_2S_5$ and $Ba_6Sn_7S_{20}$, were obtained in this work. The synthesis, crystal structures, and characterization of them are also introduced in this paper.

EXPERIMENTAL SECTION

Syntheses. Single crystals of $Ba_7Sn_5S_{15}$, $BaSn_2S_5$, and $Ba_6Sn_7S_{20}$ were synthesized by using a conventional high-temperature solid-state reaction method in the evacuated silica tubes. The starting reactants were used without further purification. BaS (99.7%) was purchased from Alfa Aesar China (Tianjin) Co., Ltd. Sn (5N) and S (99.5%) were purchased from Sinopharm Chemical Reagent Co., Ltd.

$Ba_7Sn_5S_{15}$. Crystals of $Ba_7Sn_5S_{15}$ were prepared with the molar ratio of 7:5:15 Ba/Sn/S, and 2.75 mmol of BaS, 1.96 mmol of Sn, and 3.15 mmol of S were mixed roughly. The sample was transferred into a predried graphite crucible and flame-sealed in an evacuated silica tube under 10^{-2} Pa. The tube was then placed in a temperature-controlled resistance furnace and heated to 1073 K within 50 h (holding for 30 h), and the sample was slowly cooled to 773 K in 150 h, followed by cooling to room temperature in 50 h. Bulk crystals with a red color

Received: August 20, 2012
Published: December 20, 2012

   dx.doi.org/10.1021/ic301804n | Inorg. Chem. 2013, 52, 273−279

Table 1. Crystal Data and Structural Refinement Details for Compounds $Ba_7Sn_5S_{15}$, $BaSn_2S_5$, and $Ba_6Sn_7S_{20}$

	$Ba_7Sn_5S_{15}$	$BaSn_2S_5$	$Ba_6Sn_7S_{20}$
formula weight	2035.91	535.10	2296.35
space group	$P6_3cm$	$Pccn$	$C2/c$
a (Å)	25.1234(4)	6.674(3)	24.519(9)
b (Å)	25.1234(4)	10.607(5)	6.355(2)
c (Å)	8.4120(2)	11.394(5)	23.109(8)
α (deg)	90	90	90
β (deg)	90	90	90.101(5)
γ (deg)	120	90	90
V (Å^3), Z	4598.2(2), 6	806.6(6), 4	3601(2), 4
ρ_{cal} (g cm^{-3})	4.411	4.407	4.236
abs corrn	multiscan	multiscan	multiscan
abs coeff (mm^{-1})	13.842	12.165	12.364
cryst size (mm)	0.18 × 0.16 × 0.15	0.18 × 0.16 × 0.15	0.20 × 0.18 × 0.14
F(000)	5292	944	4024.0
$R1^a$, $wR2^b$, for $I > 2\sigma(I)$	0.0349, 0.0904	0.0238, 0.0893	0.0188, 0.0340
$R1^a$, $wR2^b$, for all data	0.0357, 0.0912	0.0305, 0.1355	0.0255, 0.0357
GOF on F^2	1.010	1.044	1.014

$^aR1 = \sum||F_o| - |F_c||/\sum|F_o|$. $^bwR2(F_o^2) = [\sum w(F_o^2 - F_c^2)^2/\sum w(F_o^2)^2]^{1/2}$.

were obtained. The compounds were stable in air and moisture conditions. The energy-dispersive spectrometry (EDS) elemental analyses on single crystals of $Ba_7Sn_5S_{15}$ confirmed the Ba/Sn/S molar ratio of 1.29:1.01:2.71, which was in reasonable agreement with the stoichiometric proportions from single-crystal X-ray structural analyses.

$BaSn_2S_5$. Crystals of the compound were prepared with the molar ratio of 1:2:5 Ba/Sn/S, and 0.93 mmol of BaS, 1.87 mmol of Sn, and 3.74 mmol of S were mixed roughly. The sample was transferred into a predried graphite crucible, which was subsequently placed into a silica tube, and then sealed under 10^{-2} Pa. The synthesis procedure was similar to that of compound $Ba_7Sn_5S_{15}$ except that the highest temperature was set at 1023 K. As the temperature decreased, bulk crystals with a yellow color, which were stable in air and moisture conditions, were obtained. The EDS elemental analyses on single crystals of $BaSn_2S_5$ confirmed the Ba/Sn/S molar ratio of 1.06:2.02:5.26, which was in good agreement with the stoichiometric proportions from single-crystal X-ray structural analyses.

$Ba_6Sn_7S_{20}$. The compound was prepared with the molar ratio of 6:7:20 Ba/Sn/S, and 1.31 mmol of BaS, 1.52 mmol of Sn, and 3.04 mmol of S were mixed roughly. The mixture was transferred into a predried graphite crucible and subsequently flame-sealed in an evacuated silica tube under 10^{-2} Pa. The synthesis procedure was similar to that of $Ba_7Sn_5S_{15}$ except that the highest temperature was set at 973 K. After cooling to room temperature, a lot of bulk crystals with a yellow color were obtained. The crystals were stable in air and moisture conditions. The EDS elemental analyses on single crystals of $Ba_6Sn_7S_{20}$ confirmed the Ba/Sn/S molar ratio of 1.03:1.27:2.97, which matched well with the stoichiometric proportions from single-crystal X-ray structural analyses.

X-ray Crystallography. Single crystals of the compounds $Ba_7Sn_5S_{15}$, $BaSn_2S_5$, and $Ba_6Sn_7S_{20}$ were selected for indexing and intensity data collection. They were measured on Saturn70, Saturn724+, and Saturn70 diffractometers equipped with a graphite-monochromated Mo Kα radiation (λ = 0.71073 Å) at the temperature of 293 K, respectively. The diffraction image collection and the area detector data process were obtained with the Rigaku CrystalClear (version 1.4) program package. Polarization effects, Lorentz, and semiempirical corrections were applied to the intensity data.

All of the three crystal structures were solved by the direct methods, and refined by full-matrix least-squares fitting on F^2 by the SHELXL-97 program.[18] Space groups were determined by the systematic absence condition of the collected data. The final refined solutions were checked with the program PLATON,[19] and no higher symmetry elements were found. Detailed crystallographic data and structural refinements information are given in Table 1. The atomic coordinates and equivalent isotropic thermal parameters and selected bond distances for $Ba_7Sn_5S_{15}$, $BaSn_2S_5$, and $Ba_6Sn_7S_{20}$ are listed in Tables S1 and S2 in the Supporting Information.

The powder X-ray diffraction (PXRD) patterns were recorded on a Rigaku MiniFlex II diffractometer with Cu Kα radiation. The 2θ scanning range was 5−85° in a step size of 0.02°. The experimental and simulated PXRD patterns of $Ba_7Sn_5S_{15}$ and $BaSn_2S_5$ are shown in Figure S1 in the Supporting Information.

Second-Harmonic Generation (SHG) Measurements. The SHG response tests of $Ba_7Sn_5S_{15}$ were performed on powder samples by using the Kurtz and Perry method with a 2.05 μm Q-switch laser.[20] The SHG intensity of $Ba_7Sn_5S_{15}$ was compared with that of $AgGaS_2$, which was a representative NLO material for IR applications. Both the samples were measured in the same particle size ranges of 25−45, 45−75, 75−109, 109−150, and 150−212 μm in order to make comparisons. The samples were sieved and pressed into disks with diameters of 8 mm. Larger $AgGaS_2$ crystals were crushed, ground, and sieved into the same size range as the reference. The measurements were performed at the identical laser settings.

Infrared and UV−vis-NIR Diffuse Reflectance Spectra. The infrared spectra of the compounds were recorded on a PerkinElmer Spectrum One FR-IR spectrometer in the range of 400−4000 cm^{-1} at room temperature. The samples and dry KBr were mixed with a mass ratio of about 1:100 and ground into fine powder, then pressed into transparent sheets on the tablet machine. The prepared sheets were put in the sample chamber of the infrared spectrophotometer, and the infrared spectra were measured.

The UV−vis diffuse reflectance spectra were recorded on a PerkinElmer Lambda 900 UV−vis spectrometer in the range of 300−2500 nm at room temperature. The $BaSO_4$ plate was used as the reference material. The optical absorption spectra were converted from diffuse reflectance spectra using the Kubelka−Munk function, $\alpha/S = (1 - R)^2/2R$, where R is the scattering coefficient, and α is the Kubelka−Munk absorption coefficient.[21]

Theoretical Calculation. Energy band structure and optical properties of $Ba_7Sn_5S_{15}$ were accomplished by using DFT (density functional theory) calculation with the CASTEP code[22] provided by Material Studio package. Interaction of the electrons with ion cores was represented by the norm-conserving pseudopotentials, and the valence electrons were treated as Ba $5s^25p^66s^2$, Sn $5s^25p^2$, and S $3s^23p^4$. Generalized gradient approximation (GGA) in the scheme of Perdew−Burke−Ernzerhof (PBE) was used to describe the exchange and correlative potential of electron−electron interactions. The k-point of the first Brillouin zone was sampled as a 1 × 1 × 2 Monkhorst−Pack scheme. The energy cutoff and precision were set to be 400 eV and 2.0 × 10^{-5} eV/atom, respectively. The X-ray crystal

dx.doi.org/10.1021/ic301804n | Inorg. Chem. 2013, 52, 273−279

structure data were used without further optimization. The splitting S atom was treated as a single S atom at the middle point of the two split sites.

The calculations of optical properties in terms of the complex dielectric function $\varepsilon(\omega) = \varepsilon_1(\omega) + i\varepsilon_2(\omega)$ are given by

$$\varepsilon_2^{ij}(\omega) = \frac{8\pi^2\hbar^2e^2}{m^2V_{\text{eff}}}\Sigma_k\Sigma_{cv}(f_c - f_v)\frac{p_{cv}^i(k)p_{vc}^j(k)}{E_{vc}^2}\delta[E_{cv}(k) - \hbar\omega] \quad (1)$$

where $\delta[E_{cv}(k) - \hbar\omega] = \delta[E_c(k) - E_v(k) - \hbar\omega]$ denotes the energy difference between the conduction and valence bands at the k point with absorption of a quantum $\hbar\omega$. The f_c and f_v represent the Fermi distribution functions of the conduction and valence bands, respectively. The term $p_{cv}^i(k)$ denotes the momentum matrix element transition from the energy level c of the conduction band to the level v of the valence band at the k point in the Brillouin zones, and V is the volume of the unit cell. The m, e, and $\hbar$ are the electron mass, charge, and Plank's constant, respectively. The first-order susceptibility at the low-frequency region is given by $\chi^{(1)}(\omega)_{ii} = [\varepsilon(\omega)_i - 1]/4\pi$. The second-order susceptibilities can be expressed in terms of the first-order susceptibilities as follows

$$\chi_{ijk}^{(2)}(-\omega_3; \omega_1, \omega_2) = F^{(2)}\chi_{ii}^{(1)}(\omega_3)\chi_{jj}^{(1)}(\omega_1)\chi_{kk}^{(1)}(\omega_2) \quad (2)$$

where $F^{(2)} = ma/(N^2e^3)$. These expressions are derived from a classical anharmonic oscillator (AHO) model.[23] The m and e are, respectively, the electron mass and charge, and the parameter a, which characterizes the nonlinearity of the response and is estimated as ω_0^2/d, where d is the lattice constant and ω_0 is the vibration frequency. The N is the density number of the unit cell. For $Ba_7Sn_5S_{15}$, F is estimated to be 5.508×10^{-6} esu or 2.305×10^3 pm/V, accordingly. The SHG components d_{ij} is equal to half of the corresponding χ_{ij} value for the consequence of historical convention.

The dipole moment of the $[Sn_2S_3]^{2-}$ group was calculated by using the ab initio method with the Guassian 03 package.[24] The basis set was 6-31+G* for the S atom, and the LANL2DZ was used for the Sn atom. The geometry of $[Sn_2S_3]^{2-}$ was taken from X-ray data, and no future optimization was applied.

RESULTS AND DISCUSSIONS

Structure Description. *$Ba_7Sn_5S_{15}$.* $Ba_7Sn_5S_{15}$ crystallizes in the noncentrosymmetric space group $P6_3cm$ of the hexagonal system, with unit cell parameters of $a = b = 25.1234(4)$ Å, $c = 8.4120(2)$ Å, and $Z = 6$. There are six crystallographically unique Ba atoms, four Sn atoms, and nine S atoms in the asymmetric unit.

The coordination number of Ba(1), Ba(2), Ba(3), Ba(4), Ba(5), and Ba(6) with S atoms is 8, 8, 7, 9, 6, and 6, respectively. The Ba−S bond lengths (Table S2, Supporting Information) range from 3.030(19) to 3.590(18) Å. The Sn(1) and Sn(2) atoms are coordinated to a tetrahedron, respectively. The Sn(3) and Sn(4) atoms are simultaneously coordinated with three S atoms (bridging ligands) to form a trigonal bipyramidal. In the SnS_4 tetrahedron, Sn−S distances vary from 2.361 to 2.407 Å. The calculated bond valence sum (BVS) of 4.27 or 4.14 (Table S2, Supporting Information) is close to the oxidation state +4 of Sn.[25,26] In general, the Sn^{4+} is a 4-fold coordination cation by four S^{2-} ions, which was reported in Ba_2SnS_4 and $Ba_3Sn_2S_7$ compounds.[27,28] The stereoscopic view of the structure (Figure 1a) shows that the arrangements of the isolated $[SnS_4]^{4-}$ tetrahedra and $[Sn_2S_3]^{2-}$ trigonal bipyramids are held together by the Ba^{2+} cation. In the trigonal-bipyramidal Sn_2S_3, the oxidation state of each Sn is +2. The Sn^{2+} is a 3-fold coordination with Sn−S distances ranging from 2.583 to 2.687 Å, and the calculated BVS of 2.30 or 2.25 (Table S2, Supporting Information) is also close to oxidation state of +2. The Sn^{2+} cation is out of the triangular face of S^{2-} ions so that it is only bonded to three S^{2-} ions, and the Sn^{2+} ions can be considered to have a tetragonal environment in which a lone electron pair occupies a vertex (Figure 1b). The 3-fold coordinate structure of Sn^{2+} was reported in $BaSnS_2$, $BaSn_2S_3$, and $BaSn_3S_4$ compounds.[29−31] However, as we know, the coexistence of the 3-fold and 4-fold coordinate structures of the Sn ion in one inorganic compound has not yet been reported until this work. All of the atoms are fully sited on the Wyckoff positions with no disordered atom occupancy except S(2). The S(2) atom is split into two positions with an equivalent occupation of 50% with the total occupation of 1.

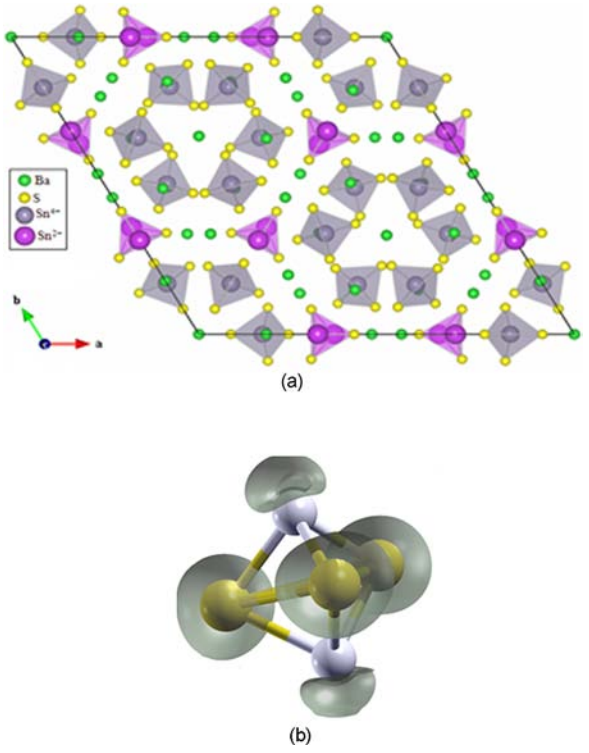

Figure 1. (a) Structure of hexagonal $Ba_7Sn_5S_{15}$ viewed down the c axis. Only half of the S(2) atoms are exhibited because of the 50% occupancy. The Ba−S bonds are not displayed for the sake of clarity. Green, pink, blue-gray, and yellow balls represent Ba, Sn(2+), Sn(4+), and S. (b) The Sn tetragonal environment with a lone electron pair occupying a vertex in the $[Sn_2S_3]^{2-}$ group.

$BaSn_2S_5$. $BaSn_2S_5$ crystallizes in the centrosymmetric space group $Pccn$ of the orthorhombic system with unit cell parameters of $a = 6.674(3)$ Å, $b = 10.607(5)$ Å, $c = 11.394(5)$ Å, and $Z = 4$. There are one crystallographically unique Ba atom, one Sn atom, and three S atoms in the asymmetric unit. The Ba atoms are coordinated by 10 S atoms. The Ba−S bond lengths (Table S2, Supporting Information) range from 3.1964(19) to 3.5393(18) Å. The Sn atoms are coordinated by five S atoms to form a SnS_5 trigonal bipyramid. The Sn−S bond lengths (Table S2, Supporting Information) range from 2.421(4) to 2.596(3) Å. Moreover, the BVS calculations give the oxidation states of 2.008 and 3.9189 for Ba^{2+} and Sn^{4+}, respectively, which are in good agreement with the structural formula (Table S2, Supporting Information).

The structure of $BaSn_2S_5$ is shown in Figure 2. The basic structural unit of SnS_5 is a trigonal bipyramid, which is connected to each other by edge sharing (Figure 2a), and forms an infinite one-dimensional $^1{}_\infty[SnS_5]^{6-}$ anionic chain. These

dx.doi.org/10.1021/ic301804n | Inorg. Chem. 2013, 52, 273−279

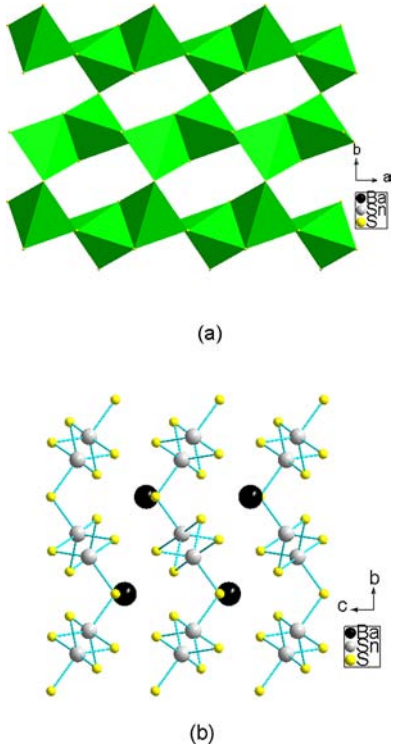

Figure 2. (a) The structure of the SnS_5 (green) trigonal bipyramid in the compound $BaSn_2S_5$ viewed down the *c* axis. (b) The crystal structure of $BaSn_2S_5$ viewed down the *a* axis. Black, gray, and yellow balls represent Ba, Sn, and S.

paralleled $^1{}_\infty[SnS_5]^{6-}$ anionic chains are connected to each other by sharing the corner of the SnS_5 trigonal bipyramid along the *a* axis direction and form the two-dimensional layer perpendicular to the *c* axis. The neighboring layers further arrange along the *c* axis, with the Ba cations in the cavities for electric charge balances, and form the whole crystal architecture (Figure 2b).

$Ba_6Sn_7S_{20}$. $Ba_6Sn_7S_{20}$ crystallizes in the centrosymmetric space group *C*2/*c* of the monoclinic system with unit cell parameters of $a = 24.519(9)$ Å, $b = 6.355(2)$ Å, $c = 23.109(8)$ Å, $\beta = 90.101(5)°$, and $Z = 4$. There are 3 crystallographically unique Ba atoms, 4 Sn atoms, and 10 S atoms in the asymmetric unit. Ba(1), Ba(2), and Ba(3) are coordinated by eight, nine and eight nearest S atoms, respectively. The Ba−S bond lengths (Table S2, Supporting Information) range from 3.0895(13) to 3.6551(14) Å. For the Sn atoms, the Sn(1) and Sn(4) are coordinated to a trigonal bipyramid by five S atoms, respectively; while the Sn(2) and Sn(3) are separately coordinated by four S atoms to form tetrahedrons. The Sn−S bond lengths (Table S2, Supporting Information) range from 2.3269(12) to 2.8115(12) Å. Moreover, the oxidation states calculationed from BVS are in reasonable agreement with the assigned ones of +2 and +4 for Ba and Sn cations in the structural formula (Table S2, Supporting Information).

The structure of $Ba_6Sn_7S_{20}$ is shown in Figure 3. There are two kinds of Sn−S polyhedrons that are a SnS_4 tetrahedron and SnS_5 trigonal bipyramid polyhedrons. Three SnS_4 tetrahedrons are connected to each other by corner sharing to form the basic structural unit $[Sn_3S_8]^{4-}$ (Figure 3a). Four SnS_5 trigonal bipyramids are connected to each other by edge sharing to form another basic structural unit, $[Sn_4S_{14}]^{12-}$. Both of the structural units $[Sn_3S_8]^{4-}$ and $[Sn_4S_{14}]^{12-}$ are connected to each other by corner sharing to form a three-dimensional framework of the $Ba_6Sn_7S_{20}$ with the Ba cations in the cavities (Figure 3b).

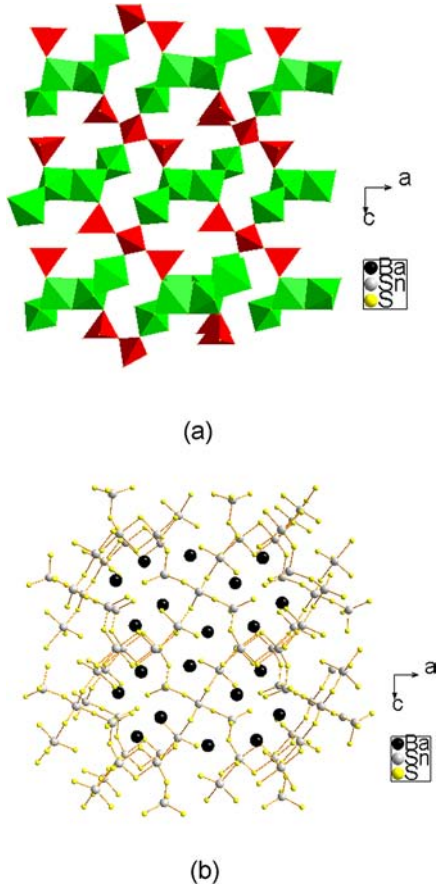

Figure 3. (a) The structure of the SnS_4 tetrahedron (red) and SnS_5 trigonal bipyramid (green) in the compound $Ba_6Sn_7S_{20}$ viewed down the *b* axis. (b) The crystal structure of $Ba_6Sn_7S_{20}$ viewed down the *b* axis. Black, gray, and yellow balls represent Ba, Sn, and S.

Thermal Analyses. Thermogravimetric analysis (TG) and differential thermal analysis (DTA) were carried out on a NETZSCH STA 449C thermal analyzer to investigate the thermal properties of the compounds $Ba_7Sn_5S_{15}$ and $BaSn_2S_5$. The samples were placed in Al_2O_3 crucibles and heated from 40 to 1000 °C at 10 °C/min in the N_2 atmosphere at a flow rate of 30 mL/min. The TG and DTA measurement results indicate that both of the compounds are thermally stable up to high temperatures. Figure S2a,b (Supporting Information) indicates that it is thermally stable up to 750 °C for the compound $Ba_7Sn_5S_{15}$ and 600 °C for $BaSn_2S_5$ under a N_2 atmosphere (Figure S2, Supporting Information).

Optical Properties. The UV−vis-NIR optical absorption spectra suggest that $Ba_7Sn_5S_{15}$ and $BaSn_2S_5$ are both semiconductors with optical band gaps of about 2.29 and 2.35 eV, respectively (Figure 4). The IR transmission spectra of $Ba_7Sn_5S_{15}$ and $BaSn_2S_5$ are shown in Figure S3 in the Supporting Information. From the figure, we can see that there are no obvious optical absorption peaks and both of the compounds exhibit a wide infrared transmission range from near-IR up to 25 μm, which covers the important band ranges of 3−5 and 8−14 μm of the atmosphere transparent windows. These results indicate that both of the compounds are the

dx.doi.org/10.1021/ic301804n | *Inorg. Chem.* 2013, 52, 273−279

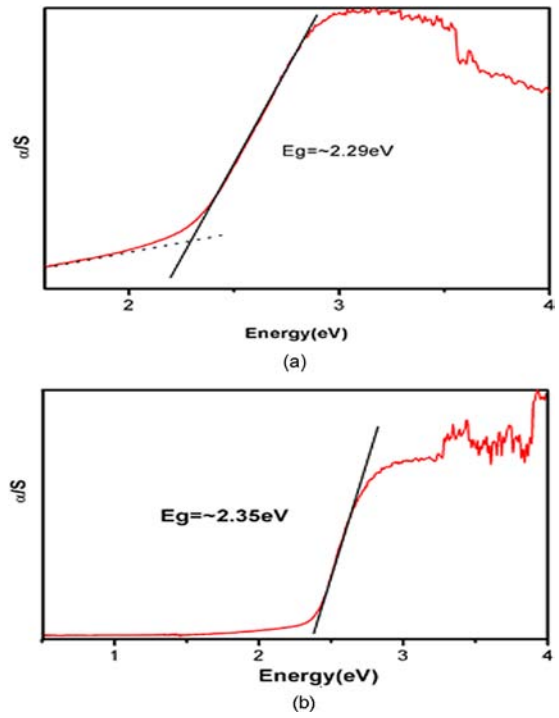

Figure 4. Optical diffuse reflectance spectra for $Ba_7Sn_5S_{15}$ (a) and $BaSn_2S_5$ (b).

potential applications to optical materials in the mid-IR ranges, especially the acentric $Ba_7Sn_5S_{15}$.

The SHG response is surveyed for the NCS compound of $Ba_7Sn_5S_{15}$. The sieved powder samples of $Ba_7Sn_5S_{15}$ (BSS) were irradiated by using a 2.05 μm Q-switched laser, and the SHG signal at 1.025 μm was detected. It was found that the SHG signal intensity of $Ba_7Sn_5S_{15}$ was about 2 times of the $AgGaS_2$ (AGS) standard of the same grain size, shown in Figure 5a. The SHG intensity depending particle size was also measured and shown in Figure 5b. It was found that, for the particle size less than 100 μm, SHG increased linearly with the particle size increasing, and for the particle size larger than 120 μm, the SHG intensity was essentially independent of particle size. This feature suggests that the compound BSS is a type-I phase matchable material based on the SHG measurements of the powder. The SHG intensity of BSS is about 10 times of that of AGS at a particle size of 30−46 μm, and about twice of that at a particle size of 150−212 μm (saturated particle size of SHG). The BSS powder nonlinear optical susceptibility, $<d_{eff}>$, can be estimated from the $<d_{eff}(BSS)> = \{I^{2\omega}(BSS)/I^{2\omega}(AGS) \times <d_{eff}(AGS)>^2\}^{1/2}$, at the same powder sizes between the BSS and the AGS and by using the same measurement system and conditions.[32] We can derive the $<d_{eff}(BSS)>$ value of 19.5 pm/V while we employ the SHG intensity ratio of 2 between the BSS and the AGS derived from Figure 5b at the saturated particle size and the $<d_{eff}(AGS)>$ value[33] of 13.9 pm/V. Here, $<d_{eff}(AGS)> = (d_{36} + d_{14} + d_{15})/3 = d_{36} = 13.9$ pm/V for the D_{2d} point group or $\bar{4}2m$ class, and $<d_{eff}(BSS)> = (4d_{31} + d_{33})/5$ for class $6mm$ under the Kleinman's symmetry condition.

Computation Section. To gain insight into the macro-and micromechanisms of the NLO effect, we calculated crystal energy band structures and molecular group electronic structures by using the first-principles method. The calculated band structures in Figure 6 show that $Ba_7Sn_5S_{15}$ is an indirect band-gap material with a gap of 2.14 eV, which is close to the

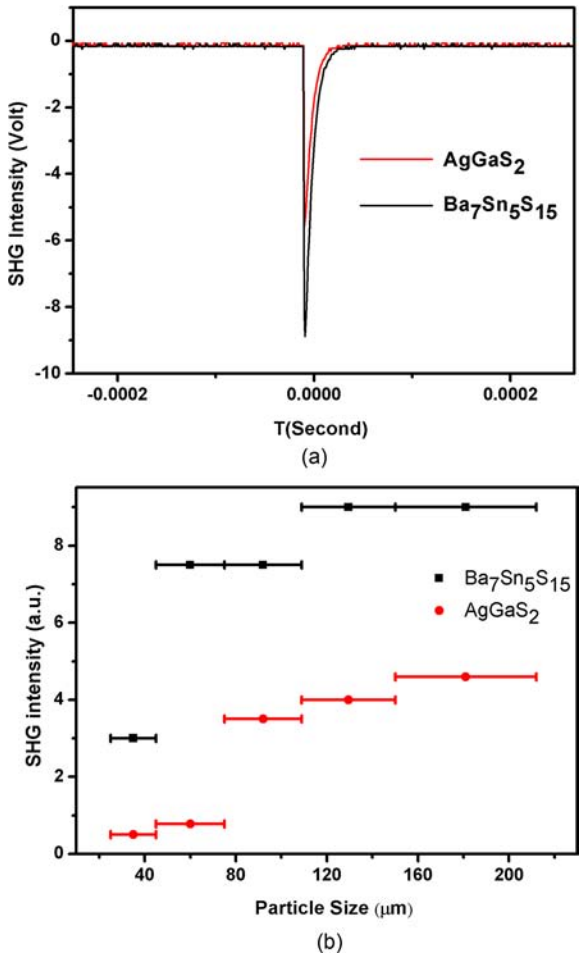

Figure 5. (a) Oscilloscope traces of the second-harmonic generated signals. (b) Phase-matching curves (i.e., particle size vs SHG intensity for $Ba_7Sn_5S_{15}$ and $AgGaS_2$).

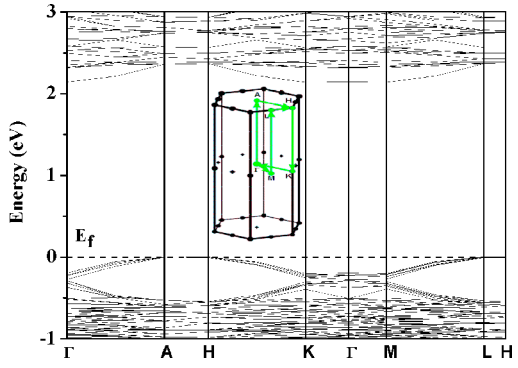

Figure 6. Energy band structure near the Fermi level for $Ba_7Sn_5S_{15}$. Inset hexahedron shows the used high symmetry k-points of first Brillouin zone.

experimental value of 2.29 eV. The calculated total and partial densities of states are plotted in Figure 7a. The band just above the Fermi level is predominately derived from Sn 5p states in group $[Sn_2S_3]^{2-}$, but has also small contributions from Sn 5s and S 3p states in group $[SnS_4]^{4-}$. However, the band just below the Fermi level is mostly composed of S 3p states in $[Sn_2S_3]^{2-}$ and $[SnS_4]^{4-}$ groups, respectively. Accordingly, the charge transfers across the band-gap edge are made within the (Sn_2S_3) and (SnS_4) polyhedrons, respectively. In views of the

dx.doi.org/10.1021/ic301804n | Inorg. Chem. 2013, 52, 273−279

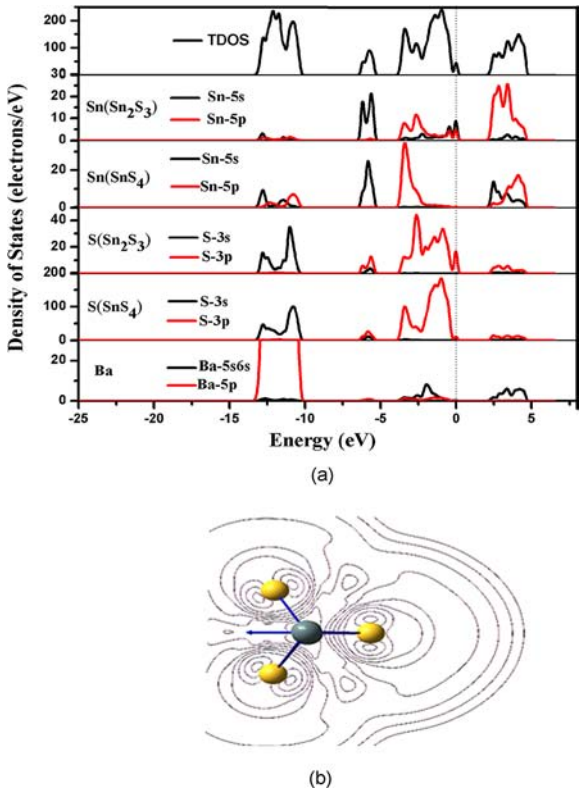

Figure 7. (a) The calculated total and partial densities of states for $Ba_7Sn_5S_{15}$ material. (b) The top view of electron density contour surface and the dipole moment for isolate $[Sn_2S_3]^{2-}$.

dipole moments of $[Sn_2S_3]^{2-}$ (2.1287 D) and $[SnS_4]^{4-}$ (0.9547 D) from the electronic structural calculations of isolate groups, we find that the polarization is much larger for the isolate trigonal-bipyramidal $[Sn_2S_3]^{2-}$ than that of the isolate distortion tetrahedral $[SnS_4]^{4-}$ in $Ba_7Sn_5S_{15}$ material. Here, we emphasize the contribution of group (Sn_2S_4) to the NLO response of $Ba_7Sn_5S_{15}$ material, although the (SnS_4) groups also have some contributions. The top view of the electron density contour surface and the dipole moment is shown in Figure 7b for isolate $[Sn_2S_3]^{2-}$, and it indicates the charge transfers from S^{2-} to Sn^{2+} ions. The arrangement of $[Sn_2S_3]^{2-}$ in the $Ba_7Sn_5S_{15}$ crystal is shown in Figure S4 in the Supporting Information, and it is found that the dipole origination of $[Sn_2S_3]^{2-}$ along the z direction is parallel to each other. The polarity superposition of the $[Sn_2S_3]^{2-}$ groups will strengthen the crystal polarity and result in a large SHG response in a crystal material of $Ba_7Sn_5S_{15}$.

The space group of $Ba_7Sn_5S_{15}$ belongs to class *6mm* and has five nonvanishing tensors of second-order susceptibility. Under the restriction of Kleinman's symmetry, only two independent SHG tensor components (d_{31} and d_{33}) were considered. The frequency-dependent SHG tensor components of the $Ba_7Sn_5S_{15}$ were calculated according to formulas 1 and 2, in which the factor F is estimated to be about 2.305×10^3 pm/V, and the calculated results are plotted in Figure S5 in the Supporting Information. The theoretical values of tensor components d_{31} and d_{33} are estimated to be about 66.9 pm/V (1.59×10^{-7} esu) and 61.9 pm/V (1.48×10^{-7} esu) at a wavelength of 2.10 μm (0.59 eV), respectively. These estimated values are larger than 3 times of the experimental value of 19.5 pm/V.

CONCLUSIONS

In summary, we have synthesized three new ternary compounds: acentric $Ba_7Sn_5S_{15}$, centric $BaSn_2S_5$, and centric $Ba_6Sn_7S_{20}$. For the centric $BaSn_2S_5$, all Sn atoms are coordinated with five S atoms to form novel SnS_5 trigonal bipyramid polyhedrons. It is worthwhile to mention that it is a kind of IR transmission material. The centric $Ba_6Sn_7S_{20}$, in which there is the coexistence of the two coordination patterns having a SnS_5 trigonal bipyramid and SnS_4 tetrahedral polyhedrons, has an uncommon crystal structure feature in the Ba−Sn−S system. In the present work, we mainly focus on the acentric $Ba_7Sn_5S_{15}$, which is a novel IR NLO crystal material with a strong SHG effect and a wide IR window. The novel structural characteristic of the (Sn_2S_3) trigonal-bipyramidal and (SnS_4) tetrahedral coordinate coexistence is first reported in the Ba−Sn−S compounds. The strong SHG effect originates from the large dipole moment of the Sn trigonal bipyramid structure, and the bipyramidal arrangements result in the polarity enhancement in the crystal structure. The crystal of $Ba_7Sn_5S_{15}$ has potential industrial applications for its features of type-I phase-match and high thermal stability.

ASSOCIATED CONTENT

Supporting Information

The experimental and simulated X-ray diffraction patterns for $Ba_7Sn_5S_{15}$ and $BaSn_2S_5$, TG and DTA curves for $Ba_7Sn_5S_{15}$ and $BaSn_2S_5$, infrared absorption spectra for $Ba_7Sn_5S_{15}$ and $BaSn_2S_5$, and CCDC reference numbers 424619, 424620, and 424621. This material is available free of charge via the Internet at http://pubs.acs.org.

AUTHOR INFORMATION

Corresponding Author

*E-mail: cwd@fjirsm.ac.cn.

Notes

The authors declare no competing financial interest.

ACKNOWLEDGMENTS

This investigation was based on work supported by the National Natural Science Foundation of China under project 21173225, the National Basic Research Program of China (No. 2007CB815307), and the Foundation of Fujian Provincial Key Laboratory of Theoretical and Computational Chemistry. We thank Prof. Ning Ye and Dr. Na Yu at FJIRSM for help with the SHG measurements.

REFERENCES

(1) Bera, T. K.; Jang, J. I.; Ketterson, J. B.; Kanatzidis, M. G. *J. Am. Chem. Soc.* **2009**, *131*, 75.

(2) Gmachl, C.; Capasso, F.; Kohler, R.; Tredicucci, A.; Hutchinson, A. L.; Sivco, D. L.; Baillargeon, J. N.; Cho, A. Y. *IEEE Circuits Devices* **2000**, *16*, 10−18.

(3) Roller, C.; Kosterev, A. A.; Tittel, F. K.; Uehara, K.; Gmachl, C.; Sivco, D. L. *Opt. Lett.* **2003**, *28*, 2052.

(4) Guo, B. J.; Wang, Y.; Peng, C.; Zhang, H. L.; Luo, G. P.; Le, H. Q.; Gmachl, C.; Sivco, D. L.; Peabody, M. L.; Cho, A. Y. *Opt. Express* **2004**, *12*, 208−219.

(5) Capasso, F.; Paiella, R.; Martini, R.; Colombelli, R.; Gmachl, C.; Myers, T. L.; Taubman, M. S.; Williams, R. M.; Bethea, C. G.; Unterrainer, K.; Hwang, H. Y.; Sivco, D. L.; Cho, A. Y.; Sergent, A. M.; Liu, H. C.; Whittaker, E. A. *IEEE J. Quantum Electron.* **2002**, *38*, 511−532.

(6) Harasaki, A.; Kato, K. *Jpn. J. Appl. Phys.* **1997**, *36*, 700−703.

(7) Eckardt, R. C.; Fan, Y. X.; Byer, R. L.; Marquardt, C. L.; Storm, M. E.; Esterowitz, L. *Appl. Phys. Lett.* **1986**, *49*, 608−610.
(8) Peterson, R. D.; Schepler, K. L.; Brown, J. L.; Schunemann, P. G. *J. Opt. Soc. Am. B* **1995**, *12*, 2142−2146.
(9) Evans, O. R.; Lin, W. *Chem. Mater.* **2001**, *13*, 2705−2712.
(10) Bells, S. D.; Ratner, M. A.; Marks, T. J. *J. Am. Chem. Soc.* **1992**, *114*, 5842−5849.
(11) Bera, T. K.; Jang, J. I.; Ketterson, J. B.; Kanatzidis, M. G. *J. Am. Chem. Soc.* **2009**, *131*, 75−77.
(12) Isaenko, L.; Vasilyeva, I.; Yelisseyev, A.; Lobanov, S.; Malakhov, V.; Dovlitova, L.; Zondy, J. J.; Kavun, I. *J. Cryst. Growth* **2000**, *218*, 313−322.
(13) Banerjee, S.; Malliakas, C. D.; Jang, J. I.; Ketterson, J. B.; Kanatzidis, M. G. *J. Am. Chem. Soc.* **2008**, *130*, 12270−12272.
(14) Isaenko, L.; Yelisseyev, A.; Lobanov, S.; Petrov, V.; Rotermund, F.; Slekys, G.; Zondy, J. J. *J. Appl. Phys.* **2002**, *91*, 9475−9480.
(15) Lin, X. S.; Zhang, G.; Ye, N. *Cryst. Growth Des.* **2009**, *9*, 1186−1189.
(16) Yao, J. Y.; Mei, D. J.; Bai, L.; Lin, Z. S.; Yin, W. L.; Fu, P. Z.; Wu, Y. C. *Inorg. Chem.* **2010**, *49*, 9212−9216.
(17) Chung, I.; Jang, J. I.; Malliakas, C. D.; Ketterson, J. B.; Kanatzidis, M. G. *J. Am. Chem. Soc.* **2010**, *132*, 384−389.
(18) Sheldrick, G. M. *SHELXTL-9*; University of Göttingen: Göttingen, Germany, 1997.
(19) Spek, A. L. *J. Appl. Crystallogr.* **2003**, *36*, 7.
(20) Hervieu, M.; Perez, G.; Hagenmuller, P. *Bull. Soc. Chim. Fr.* **1967**, *6*, 2189−2194.
(21) Wendlandt, W. W.; Hecht, H. G. *Reflectance Spectroscopy*; Interscience: New York, 1966.
(22) Clark, S. J.; Segall, M. D.; Pickard, C. J.; Hasnip, P. J.; Probert, M. J.; Refson, K.; Payne, M. C. *Z. Kristallogr.* **2005**, *220*, 567−570.
(23) Boyd, R. W. *Nonlinear Optics*; Academic Press: New York, 1992; pp 21−47.
(24) Frisch, M. J.; Trucks, G. W.; Schlegel, H. B.; Scuseria, G. E.; Robb, M. A.; Cheeseman, J. R.; Montgomery, J. A., Jr.; Vreven, T.; Kudin, K. N.; Burant, J. C.; Millam, J. M.; Iyengar, S. S.; Tomasi, J.; Barone, V.; Mennucci, B.; Cossi, M.; Scalmani, G.; Rega, N.; Petersson, G. A.; Nakatsuji, H.; Hada, M.; Ehara, M.; Toyota, K.; Fukuda, R.; Hasegawa, J.; Ishida, M.; Nakajima, T.; Honda, Y.; Kitao, O.; Nakai, H.; Klene, M.; Li, X.; Knox, J. E.; Hratchian, H. P.; Cross, J. B.; Bakken, V.; Adamo, C.; Jaramillo, J.; Gomperts, R.; Stratmann, R. E.; Yazyev, O.; Austin, A. J.; Cammi, R.; Pomelli, C.; Ochterski, J. W.; Ayala, P. Y.; Morokuma, K.; Voth, G. A.; Salvador, P.; Dannenberg, J. J.; Zakrzewski, V. G.; Dapprich, S.; Daniels, A. D.; Strain, M. C.; Farkas, O.; Malick, D. K.; Rabuck, A. D.;Raghavachari, K.; Foresman, J. B.; Ortiz, J. V.; Cui, Q.; Baboul, A. G.; Clifford, S.; Cioslowski, J.; Stefanov, B. B.; Liu, G.; Liashenko, A.; Piskorz, P.; Komaromi, I.; Martin, R. L.; Fox, D. J.; Keith, T.; Al-Laham, M. A.; Peng, C. Y.; Nanayakkara, A.; Challacombe, M.; Gill, P. M. W.; Johnson, B.; Chen, W.; Wong, M. W.; Gonzalez, C.; Pople, J. A. *Gaussian 03*, revision B; Gaussian Inc.: Pittsburgh, PA, 2003.
(25) Brese, N. E.; O'keeffe, M. *Acta Crystallogr., Sect. B* **1991**, *47*, 192−197.
(26) Jensen, W. P.; Palenik, G. J.; Tiekink, E. R. T. *Polyhedron* **2001**, *20*, 2137−2143.
(27) (a) Susa, K.; Steinfink, H. *J. Solid State Chem.* **1971**, *3*, 75−82. (b) Jumas, J. C.; Philippot, E.; Vermot-Gaud-Daniel, F.; Ribes, M.; Maurin, M. *J. Solid State Chem.* **1975**, *14*, 319−327.
(28) Jumas, J. C.; Ribes, M.; Philippot, E. *C. R. Hebd. Seances Acad. Sci., Ser. C* **1971**, *273*, 1356−1357.
(29) del Bucchia, P. S.; Jumas, J. C.; Maurin, M. *Acta Crystallogr., Sect. B* **1980**, *36*, 2935−2940.
(30) Iglesias, J. E.; Steinfink, H. *Acta Crystallogr., Sect. B* **1973**, *29*, 1480−1483.
(31) Hervieu, M.; Perez, G.; Hagenmuller, P. *Bull. Soc. Chim. Fr.* **1967**, *6*, 2189−2194.
(32) (a) Kurtz, S. K.; Perry, T. T. *J. Appl. Phys.* **1968**, *39*, 3798−3813. (b) Dougherty, J. P.; Kurtz, S. K. *J. Appl. Crystallogr.* **1976**, *9*, 145−158.
(33) Zondy, J.-J.; Touahri, D.; Acef, O. *J. Opt. Soc. Am. B* **1997**, *14*, 2481−2497.